

---

**Design, Optimization, and Experimental Study of a Novel  
Direct Driven Linear-Rotary Wave Generator**

Journal:	<i>IEEE Transactions on Energy Conversion</i>
Manuscript ID	TEC-01067-2023.R2
Manuscript Type:	Regular Research Paper (S1)
Technical Topic Area:	Tidal/wave power < Energy Development and Power Generation, Permanent magnet machinery systems < Electric Machinery
Key Words:	Wave energy converter, Linear-rotary generator, Multi-objective optimization

SCHOLARONE™  
Manuscripts

TEC-01067-2023

1

# Design, Optimization, and Experimental Study of a Novel Direct-Driven Linear-Rotary Wave Generator

Lixun Zhu, Lei Zhu, Qingyun Wu, Ting Xu, Min Huang, Ning Gao, Kangan Wang, Weimin Wu, Wei Li, *Member, IEEE*; Chang-seop Koh, *Senior Member, IEEE* and Frede Blaabjerg, *Fellow, IEEE*

**Abstract**—Direct-driven generation is considered one of the most reliable selections in wave energy conversion systems. Therefore, a direct-driven linear-rotary wave generator (LRWG), which can transfer the low-speed linear wave motion to the high-speed rotating motion of the rotor and then generate electrical power simultaneously, is proposed in this paper. The proposed LRWG comprises three parts: translator, common rotor, and stator. From the energy view, the proposed LRWG can be divided into two sections: the energy transmission section to increase the velocity of the wave and the energy conversion section to generate power. The initial design method is given to determine the main dimensions of the proposed LRWG. To meet the maximum power tracking control requirements, a multi-mode and multi-objective optimization method, which can consider both generator and motor mode, is proposed to improve the performance of the proposed LRWG by sensitivity analysis, response surface methodology, and non-dominated sorting genetic algorithm II method. Finally, a prototype and its experimental platform are developed based on one of the optimization schemes from the possible solutions to verify the proposed approach and the performance of the proposed LRWG.

**Index Terms**—Wave energy converter, Linear-rotary generator, Multi-objective optimization.

## I. INTRODUCTION

WITH the discussion on energy issues gradually heating, the green and sustainable ocean energy with high energy density, strong predictability, and low variability [1] has become a research hotspot. Up to now, although wave energy conversion technology has made good

This work was supported in part by the National Natural Science Foundation of China under Grant 52007113 and Grant 52377014, in part by Shanghai 2022 Science and Technology Innovation Action Plan-Star Cultivation (Sailing Program) under Grant 22YF1415700, and in part by the Shanghai Frontiers Science Center of “Full Penetration” Far-Reaching Offshore Ocean Energy and Power. (Corresponding authors: Qingyun Wu and Wei Li.).

Lixun Zhu, Lei Zhu, Qingyun Wu, Ting Xu, Min Huang, Ning Gao, Kangan Wang and Weimin Wu are with the Department of Electrical Engineering, Shanghai Maritime University, Shanghai 201306, China (e-mail: [lixzhu@shmtu.edu.cn](mailto:lixzhu@shmtu.edu.cn); [202430210065@stu.shmtu.edu.cn](mailto:202430210065@stu.shmtu.edu.cn); [ting.x@wustl.edu](mailto:ting.x@wustl.edu); [202130210096@stu.shmtu.edu.cn](mailto:202130210096@stu.shmtu.edu.cn); [minhuang@shmtu.edu.cn](mailto:minhuang@shmtu.edu.cn), [ngao@shmtu.edu.cn](mailto:ngao@shmtu.edu.cn); [kawan.g@shmtu.edu.cn](mailto:kawan.g@shmtu.edu.cn); [wmwu@shmtu.edu.cn](mailto:wmwu@shmtu.edu.cn)).

Wei Li is with the Department of Electrical Engineering, Tongji University, Shanghai, 201804, China (e-mail: [liwei@mail@tongji.edu.cn](mailto:liwei@mail@tongji.edu.cn)).

Chang-seop Koh is with the Department of Electrical Engineering, Chungbuk National University, Chonju 21366, Korea (e-mail: [kohcs@cbnu.ac.kr](mailto:kohcs@cbnu.ac.kr)).

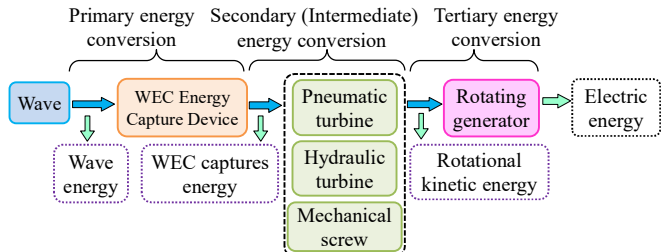
Frede Blaabjerg is with the Department of Energy Engineering, Aalborg University, Aalborg 9100, Denmark (e-mail: [fbl@et.aau.dk](mailto:fbl@et.aau.dk)).

progress, there is still a long way to go before commercialization, which is mainly because the reliability and efficiency of wave energy converter (WEC) cannot be satisfied with the harsh environment of the ocean and the particular wave motion.

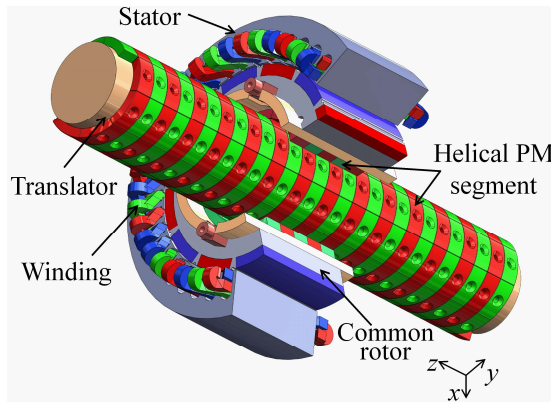
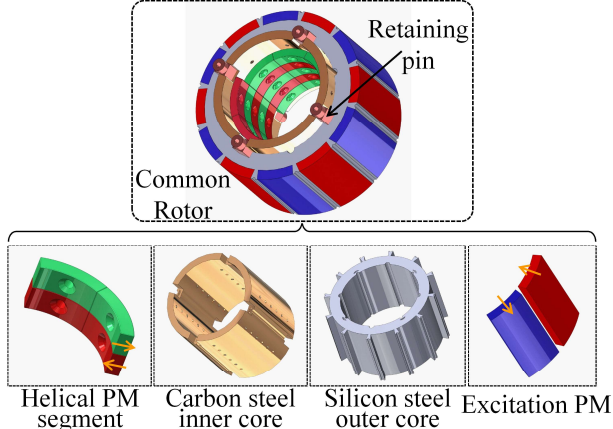
Until now, one of the most commercially promising WECs is the point-absorbing type [2], which can capture wave energy with low-speed linear motion by floating on the ocean's surface. The motion of a buoy has characteristics similar to those of a wave: high thrust, low-speed linearity, and reciprocation [3].

The existing point-absorbing type WEC can be divided into two main types: direct-driven and non-direct-driven. In a non-direct driven WEC system, an intermediate energy conversion device, such as pneumatic, hydraulic, or mechanical screw conversion devices [4], is introduced to transfer the low-speed linear motion to high-speed rotational motion. Then, the electrical power is generated by a rotational generator connected to the intermediate energy conversion device, and the energy flow path is shown in Fig. 1. Though the power density of the generator is high, the reliability is not good because of its complex structure. On the other hand, additional energy must be consumed because the pneumatic and hydraulic devices need a continuous energy supply to ensure that they can convert energy when the WEC system is running. Although the mechanical screws don't need a power supply, the contacted nut is easy to break when faced with huge wave thrust under a harsh ocean state. In addition, not only pneumatic or hydraulic transmission devices, but also mechanical screw, they all need periodic maintenance. This cost is enormous in the ocean, especially far from the shore.

A direct-driven system means no intermediate energy conversion device; a linear generator is directly connected to the buoy to generate electrical power [5]. The reliability and efficiency of the system are good. Still, the volume of the linear generator is huge when its rated power is the same as the non-direct driven system because the wave velocity is relatively low. A huge linear generator installed in the ocean



**Fig. 1.** Energy flow diagram with an intermediate energy conversion device.

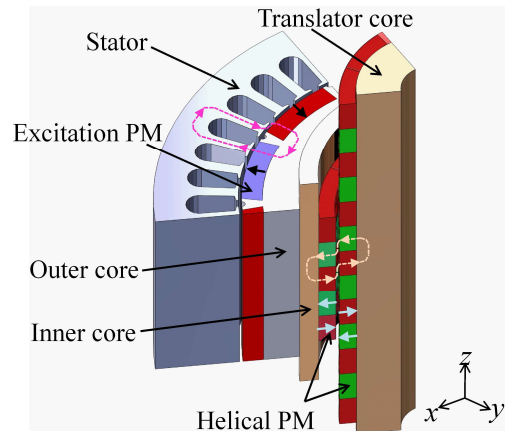
1  
2  
3  
4  
5  
6  
7  
8  
9  
10  
11  
12  
13  
14  
15  
16  
17  
TEC-01067-2023**Fig. 2.** The structure of the proposed LRWG.**Fig. 3.** Components of the common rotor.

will face great difficulty in transportation, installation, maintenance, etc.

A magnetic lead screw (MLS) is a transmission that can realize the conversion between linear motion and rotary motion using the coupling helical magnetic field in the air gap between the rotor and translator [6]-[8]. Therefore, compared with the mechanical screw, it can be applied to the WEC system to increase the power density because of its strong fault tolerance, low friction loss, and low maintenance cost. A kind of WEC based on MLS is proposed in [9]; a rotational generator is connected to the rotor of MLS by a belt. Though the reliability and efficiency of MLS are better than those of other transmission devices, they are worse than those of the direct-driven method.

Some research results have been obtained on linear-rotary motors and generators used in several applications [10]-[13]. In the wave energy conversion field, a dual stator linear-rotary generator is proposed in [13]. However, its linear and rotating generators are independent. Its power density is low because the magnetic field frequency in the air gaps is the same as that of the wave.

Based on the above, to improve the reliability and efficiency of the WEC system, a novel direct-driven linear-rotary wave generator (LRWG), which can transfer the low-speed linear motion to high-speed rotating motion and then generate electrical power simultaneously, is proposed in this paper. The proposed LRWG comprises three parts: translator, common rotor, and stator. From the energy view, the proposed LRWG can be divided into two sections: the energy transmission (ET)

**Fig. 4.** Operating principle of the proposed LRWG.

section to increase the velocity of waves and the energy conversion (EC) section to generate power. The initial design method is given to determine the main dimensions of the proposed LRWG. To meet the maximum power tracking strategy requirements, a multi-mode and multi-objective optimization method, which can consider both generator mode (GM) and motor mode (MM), is proposed to improve the performance of the proposed LRWG by sensitivity analysis, response surface methodology (RSM), and non-dominated sorting genetic algorithm II (NSGA II) method. Finally, a prototype and its experimental platform are developed based on one of the optimization schemes from the possible solutions to verify the proposed approach and the performance of the proposed LRWG.

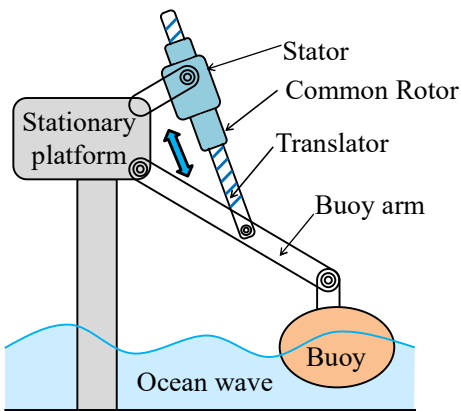
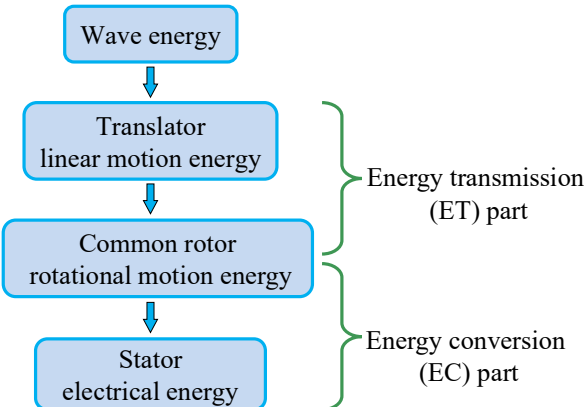
In this paper, the topology of the proposed LRWG is presented in section II, and its operating principle is analyzed. In section III, an initial design method that can consider both the ET and the EC sections is proposed, and the initial design results of the LRWG are obtained. The multi-mode and multi-objective optimization method is implemented in section IV. Based on the optimization results, the prototype of the proposed LRWG is manufactured, and its experimental platform is formed to verify its performance. Finally, the paper is concluded in section V.

## II. TOPOLOGY AND PRINCIPLE OF OPERATION

### A. Topology

The topology of the proposed LRWG is shown in Fig. 2, which comprises three parts: translator, common rotor, and stator, and they are coaxially installed with a  $z$ -axis. The core of the common rotor consists of two layers with different materials, the inner carbon steel core and the outer silicon steel core, as illustrated in Fig. 3. The two layers are connected by retaining pins to ensure that the two parts do not move relative to each other when the rotor is rotating. The helical PM with alternating opposite poles is installed on the inner surface of the rotor, which can generate a helical magnetic field and coupled with that generated by the same arranged PM on the outer surface of the translator. The PM attached to the outer surface of the rotor is used to generate the magnetic source in the EC section to generate electrical power. The material carbon steel is selected for the inner layer of the rotor because

TEC-01067-2023

**Fig. 5.** Initial design process for LRWG.**Fig. 6.** Axial cutaway view of ET section.

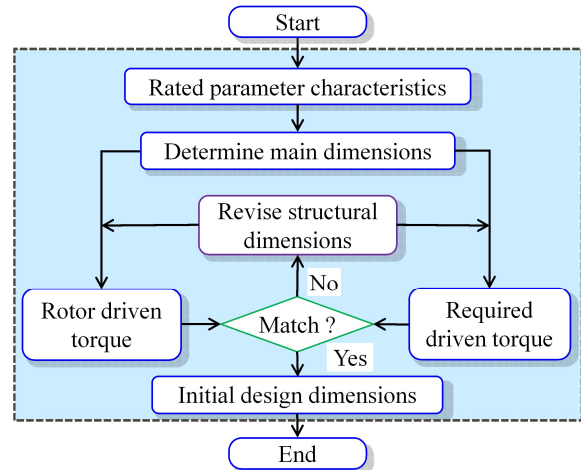
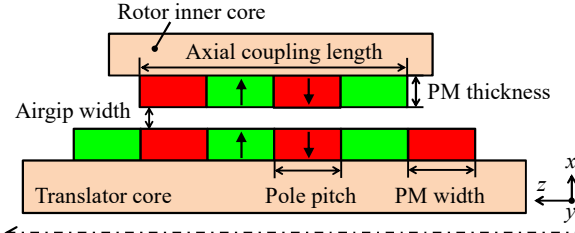
its stiffness is big enough not only to support the outer layer core but also to stand the considerable shear stress generated by the helical magnetic field between the rotor and the translator. The excitation PM and the helical PM on the rotor and translator are radially magnetized, as shown in Fig. 3.

From the energy view, the proposed LRWG can be divided into ET and EC sections. The ET section concludes the translator and the inner layer of the rotor, while the EC section concludes the stator and the outer layer of the rotor.

#### B. Operating Principle

In a point-absorbing WEC system, as shown in Fig. 5, the wave energy can be captured by the buoy. The translator of the proposed LRWG is mechanically connected to the buoy and moves following the buoy and wave. Then, through the helical coupling magnetic field in the air gap of the ET section, the torque can be generated from the thrust force of the translator to drive the rotor to rotate. The main magnet flux path of the ET section is given in Fig. 4. The energy flow chart of the proposed LRWG is shown in Fig. 6.

The translator can move up and down linearly with the buoy on the ocean's surface, and the translator's velocity is equal to that of the buoy and wave. Once the translator moves with velocity  $v$ , the energy can be transferred from the translator to the rotor through the coupling helical magnetic field in the airgap between the translator and rotor, and the rotor will rotate synchronously with velocity  $\omega$  follows the relationship

**Fig. 7.** Initial design process for LRWG.**Fig. 8.** Axial cutaway view of ET section.

shown in (1) based on the energy conservation law when neglecting the transmission loss [7], as:

$$\begin{cases} F_t / T_r = \omega / v = 2\pi / \lambda = G \\ \lambda = 2p\tau_p \end{cases} \quad (3a)$$

where  $F_t$  and  $T_r$  are, respectively, the axial thrust force of the translator and the driven torque of the rotor,  $\lambda$  is the transmission lead, defined as the distance that the translator moves synchronously when the rotor rotates one revolution.  $p$  and  $\tau_p$  are the number of pole pairs and the pole pitch of the helical magnetic poles, respectively.

As the rotor rotates, the energy can be transferred to the stator and generate electrical power through the rotating magnetic field in the air gap between the rotor and the stator in the EC section. Therefore, the driven torque of rotor  $T_r$  should satisfy the following condition:

$$T_r \geq T_e + T_0 + \sigma \quad (\sigma > 0) \quad (3a)$$

where  $T_0$  is the no-load torque, and  $\sigma$  is the driven torque margin, which is a value that changes as the rated power of the proposed LRWG.

### III. INITIAL DESIGN OF THE PROPOSED LRWG

#### A. Initial Design Process

To determine the main dimensions of the proposed LRWG, the initial design process, which should consider both ET and EC sections together, is proposed as follows, and the corresponding flow chart is shown in Fig. 7:

- Step 1: Determine the rated parameters.

1  
2  
3 TEC-01067-2023  
4  
5  
6  
7  
8  
9  
10  
11  
12  
13  
14

- 2) Step 2: Determine the main dimensions according to the rated parameters, which include the length of the translator and the outer diameter of the stator.
- 3) Step 3: Calculate the required driven torque of the rotor.
- 4) Step 4: Determine the effective PM length of the rotor's inner surface and the translator's outer diameter.
- 5) Step 5: Calculate the maximum driven torque of the rotor in the ET section.
- 6) Step 6: Cycling from step 3 to step 5 to adjust all results until the torque requirement is met.
- 7) Step 7: Determine the results of the initial dimensions.

#### B. Design of the ET Section

##### 1) Rotor Driven Torque Calculation

The driven torque of the rotor can be calculated based on the semi-analytical method [14]:

$$T_r = K_a \frac{r_a^2}{\mu_0} \int_0^{l_z} \int_0^{2\pi} B_{ra} B_{\theta a} d\theta dz = K_a \mu_0 p \tau_p l_z \sum_{n=1}^{\infty} (b_n c_n - a_n d_n) \quad (3a)$$

$$K_a = (S_c - S_h) / S_c = 1 - \frac{N_s r_a^2}{2 R_a \tau_p} \quad (3b)$$

where  $\mu_0$  is the magnetic permeability of air,  $r_a$  is the average airgap radius between the translator and rotor, and  $l_z$  is the axial coupling length of the rotor.  $B_{ra}$  and  $B_{\theta a}$  are the radial and circumferential components of the magnetic flux density, respectively.  $a_n$ ,  $b_n$ ,  $c_n$ , and  $d_n$  are the Fourier transform coefficients of the magnetic flux density.

##### 2) Structural Design and Analysis

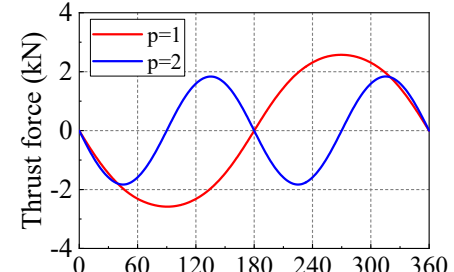
To design the ET section of the proposed LRWG, the number of pole pairs, core material and the helical shape PM assemble method should be determined. In this part, the ET

35 TABLE I  
36 THE SPECIFICATION OF THE ET SECTION

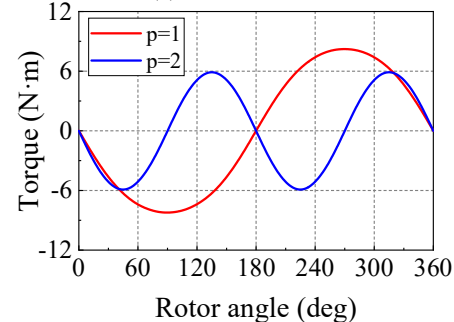
Quantity (unit)	Value
Radius of translator core (mm)	20
Thickness of rotor inner core (mm)	8
Axial coupling length of helical PM (mm)	60
Helical PM thickness (mm)	5
Airgap width (mm)	1
Core material for ET section	C45E4
Material for helical PM	NdFe35
Remanent flux density of helical PM (T)	1.23
Relative recoil permeability of helical PM	1.1
Pole pitch (mm)	$p=1$ 10 $p=2$ 5
Helical PM width (mm)	$p=1$ 10 $p=2$ 5

51 TABLE II  
52 THE RATED PARAMETERS OF THE LRWG

Symbol	Quantity (unit)	Value
$P_{out}$	Rated output power (W)	400
$n_N$	Rated rotor speed (rpm)	500
$v_N$	Rated translator speed (m/s)	0.167
$I_N$	Rated current (A)	2.2
$U_N$	Rated voltage (V)	60
$f_N$	Rated frequency (Hz)	50



(a) Thrust force.



(b) Torque.

Fig. 9. Thrust force and torque at different pole-pair numbers.

section is analyzed by the finite element method (FEM) based on the specifications listed in Table I to analyse the above problems. The structural parameters of the ET section are shown in Fig. 8.

##### a) Pole Pair Determination

The thrust force and torque corresponding to the different pole pairs are compared in Fig. 9. It can be observed that the peak values of thrust force and torque are slightly larger at  $p=1$  than at  $p=2$ , which indicates that the PM utilization when  $p=1$  is higher. Also, the force period at  $p=1$  is twice as long as at  $p=2$ . And the stability when  $p=1$  is better than that when  $p=2$ . In summary, a smaller number of pole pairs has some advantages, so the number of pole pairs in the ET section is chosen to be 1.

##### b) Core Material Determination

Theoretically, silicon steel is a good choice for the inner core of the rotor [15]. However, if the whole rotor is made of silicon steel, the stiffness of the rotor cannot withstand the driven torque, and the helical PM is difficult to install. Therefore, carbon steel is selected for the inner layer of the rotor because of its higher stiffness.

The magnetic field distribution and thrust force of the ET section corresponding to the two materials are compared in Fig. 10. It can be observed that there is a good agreement between the performances of the two materials, which is mainly due to the fact that the magnetic flux is not saturated, as can be derived by comparing the B-H curve shown in Fig. 10(d).

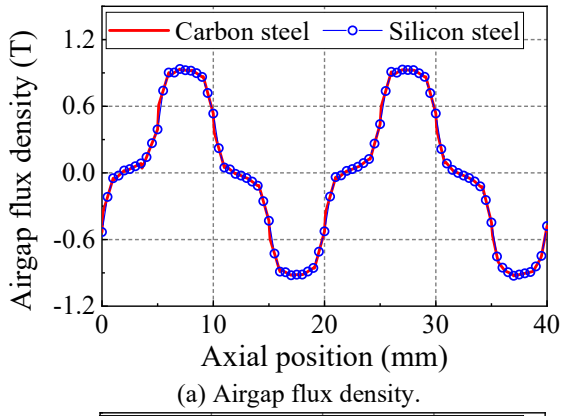
##### c) Assembly of Helical PM Segment

The traditional installation method of the helical PM is to fix it with metal glue after segmentation [16]. The method is simple, but accuracy cannot be guaranteed. The PM segments

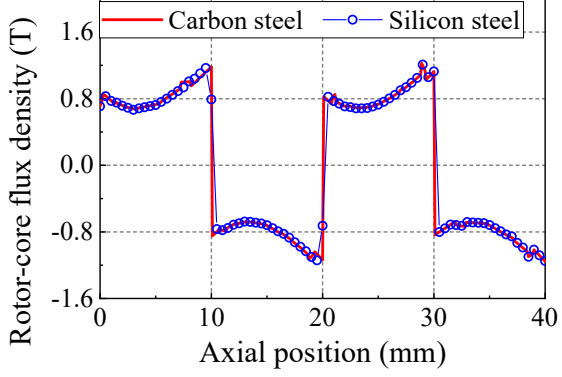
TEC-01067-2023

can not be replaced once they are demagnetized and damaged.

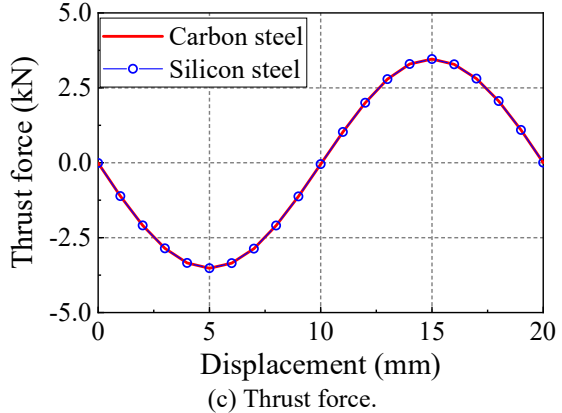
To solve this problem, the proposed LRWG's helical PM adopts a novel bolting method. The assembly of the helical



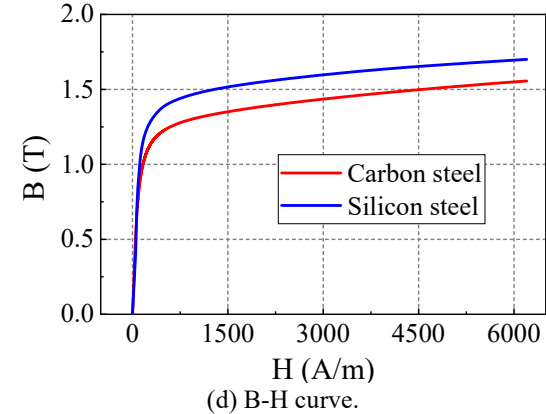
(a) Airgap flux density.



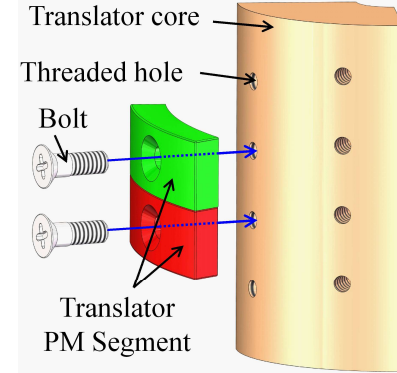
(b) Rotor core flux density.



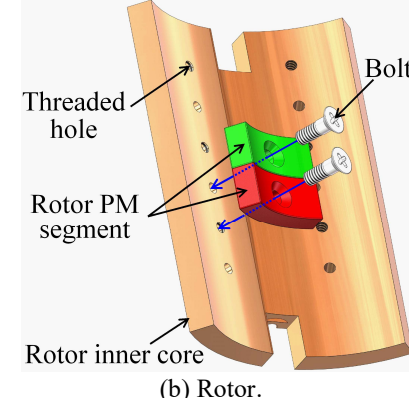
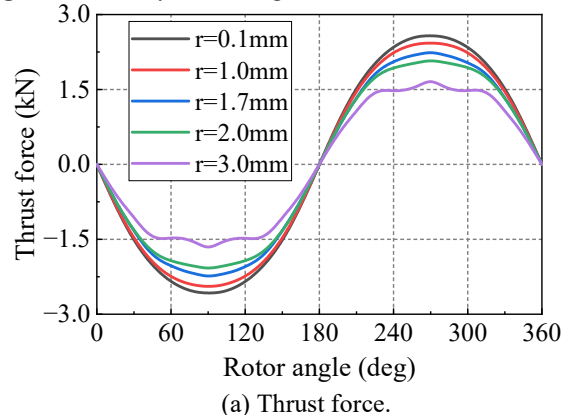
(c) Thrust force.



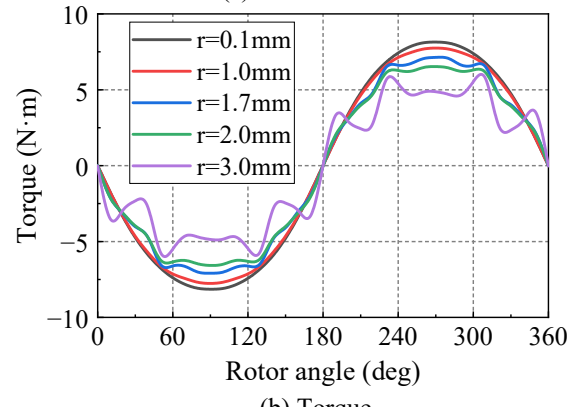
(d) B-H curve.

**Fig. 10.** Comparisons with two types of core materials.

(a) Translator

**Fig. 11.** Assembly of PM segments.

(a) Thrust force.



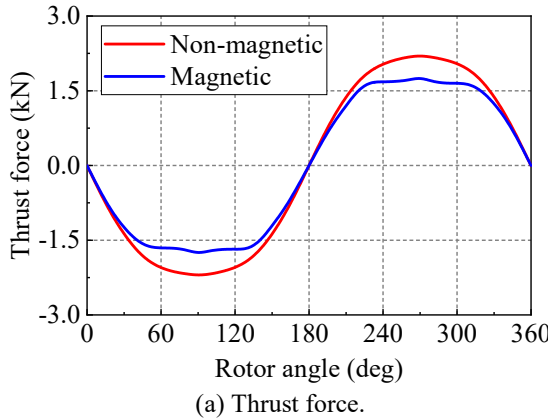
(b) Torque.

**Fig. 12.** Effect of hole radius of helical PM.

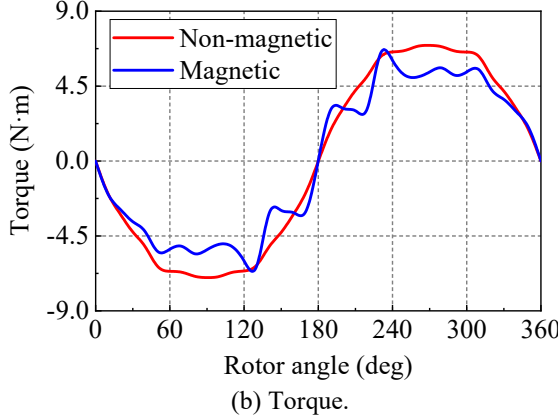
1  
2 TEC-01067-2023  
3  
4

5 PM segments is shown in Fig. 11.  
6

7 Through FEM, the effects of the radius of the penetration  
8 holes in the PM segments on the thrust force and torque of the  
9 ET section are given in Fig. 12. It can be seen that as the  
10 radius of the penetration holes increases, the peak values of  
11



(a) Thrust force.



(b) Torque.

Fig. 13. Effect of bolt material on thrust force and torque.

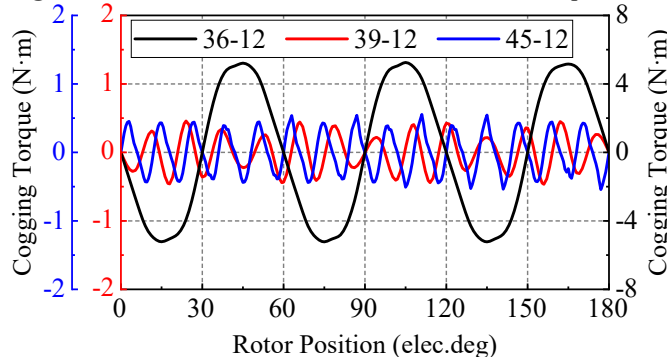


Fig. 14. The cogging torque corresponding to different slot pole combinations.

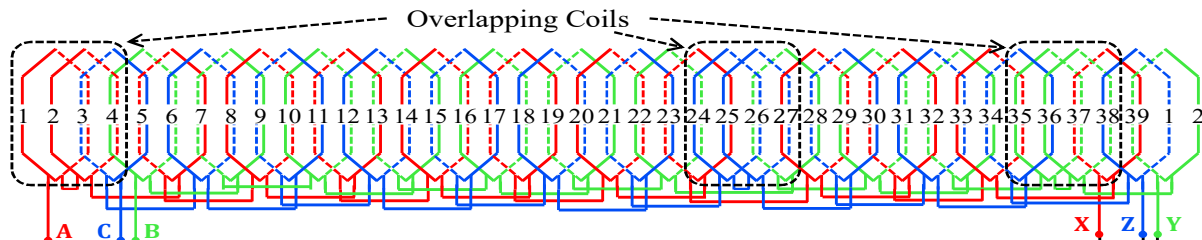


Fig. 15. winding distribution.

force gradually decrease and due to higher harmonic because the distortion of the magnetic field distribution in the airgap. To balance the performance between the bearing force of the bolts and transmission performance, the radius of the penetration hole is taken as 1.7 mm.

The effects of magnetic and non-magnetic bolts on the force performances are given in Fig. 13. The results show that the ET section corresponding to the non-magnetic bolt performs better. Therefore, non-magnetic bolts made of stainless steel

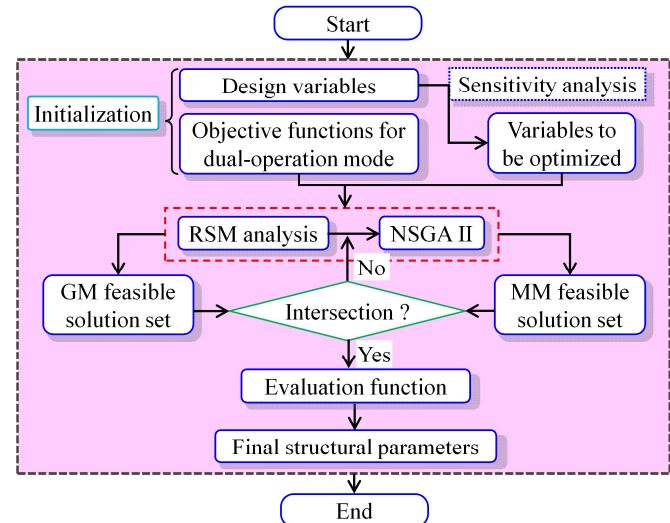
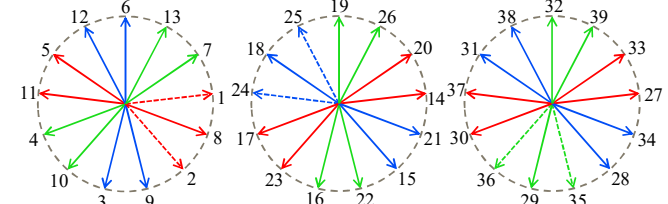
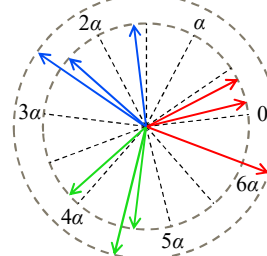


Fig. 16. Multi-objective optimization process for LRWG.



(a) Slot potential star diagram.



(b) Synthesis of slot potentials.

Fig. 17. Slot potential star diagram

TEC-01067-2023

have been chosen.

### C. Design of the EC Section

#### 1) Basic Dimension

The function of the stator is to output the electrical power of LRWG, so the relationship between rated the electrical power and stator dimension is as follows:

$$R_{si}^2 L_s = \frac{60(P_e - p_{Cu})}{\sqrt{2}\pi^3 n_N K_w \alpha_p B_g A_w K_e \cos \varphi_N} \quad (3a)$$

where  $R_{si}$  is the inner radius of the stator,  $n_N$  is the rated speed of the rotor,  $B_g$  is the magnetic load,  $A_w$  is the line load,  $\alpha_p$  is the pole arc coefficient,  $K_w$  is the winding coefficient,  $K_e$  is the voltage coefficient,  $\varphi_N$  is the power factor angle, and  $p_{Cu}$  is the copper loss.

The following formulas can obtain the outer radius  $R_{so}$  and length  $L_s$  of the stator:

$$L_s = 2\lambda_a R_{si}, \quad R_{so} = R_{si} / \lambda_w \quad (3a)$$

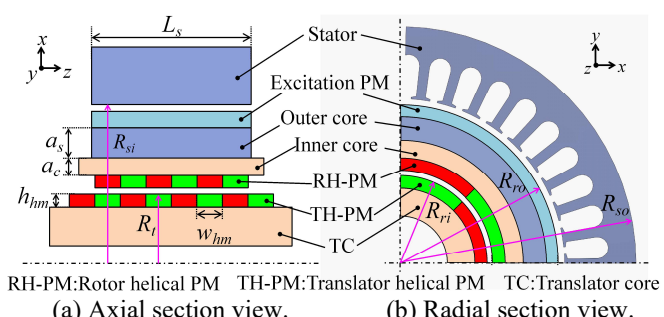
where  $\lambda_a$  and  $\lambda_w$  are the ratio of length to inner diameter and the ratio of outer and inner diameters of the stator, respectively.

#### 2) Matching of Slots and Poles

For the proposed LRWG, reducing the cogging torque is one of the necessary design goals related to its start and control performance. From the perspective of energy [16], the cogging torque can be expressed as:

$$T_{cog}(\theta) = \frac{\pi Q L_s}{4\mu_0} (R_{sy}^2 - R_{st}^2) \sum_{n=1}^{\infty} n G_n B_m \sin(nQ\theta) \quad (3a)$$

where  $\theta$  is the angle between the pole and tooth centerline,  $Q$  is the number of stator slots, and  $R_{sy}$  is the inner radius of the stator yoke.  $B_m$  and  $G_n$  are the Fourier transform coefficients of the remanent magnetization of the excitation PM and the airgap magnetically guided wave, respectively, which only work on the cogging torque when  $nQ/2p_r$  is an integer, where  $p_r$  is the number of pole pairs of the excitation poles. The higher the order of  $nQ/2p_r$ , the faster the vibration frequency and the lower the



(a) Axial section view. (b) Radial section view.

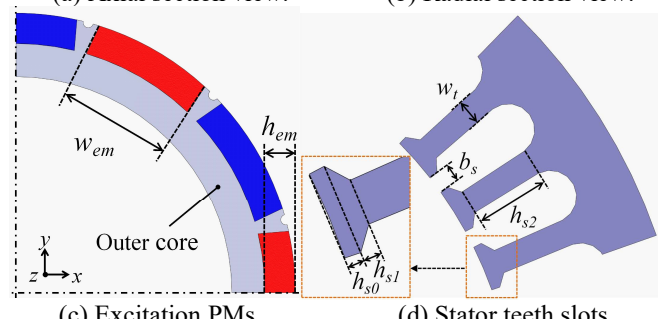


Fig. 18. Design parameters of the LRWG.

amplitude of the cogging torque corresponding to the order.

According to the above analysis and rated parameters in Table II, LRWG adopts an asymmetric combination of slots and poles with 39 and 12 poles to reduce the cogging torque. The FEM comparison results of the cogging torque under several slot pole combinations are in Fig. 14. The results show the advantage of the asymmetric slot pole combination in terms of cogging torque. The 45-slot also has good cogging torque, but the higher number of slots creates problems such as difficulty embedding coils and low ingress protection (IP) level, especially for the ocean

TABLE III  
THE SPECIFICATION OF THE LRWG

Symbol	Quantity (unit)	Value
$L_s$	Length of stator (mm)	60
$R_{so}$	Outer radius of stator (mm)	82
$R_{si}$	Inner radius of stator (mm)	56
$R_{ro}$	Outer radius of rotor (mm)	55
$R_{ri}$	Inner radius of rotor (mm)	28
$R_t$	Radius of translator (mm)	27
$g_a$	Airgap width between translator and rotor (mm)	1
$g_b$	Airgap width between rotor and stator (mm)	1
$N_c$	Winding turns	32
$\cos \varphi_N$	Power factor	0.88
$\alpha_p$	Polar arc coefficient	0.79
$K_e$	Voltage coefficient	0.9
$A_w$	Line load (A/m)	3650
$B_g$	Magnetic load (T)	1.6
$\lambda_a$	Ratio of length to inner diameter	0.54
$\lambda_w$	Ratio of inner and outer diameters	0.68

TABLE IV  
THE RATED PARAMETERS OF THE LRWG

Item	Relative Permeability	$B_{rem}$
NdFe52	1.05	1.42T

TABLE V  
THE OPTIMIZATION PARAMETERS OF THE LRWG

Symbol	Quantity (unit)	Value
$w_{hm}$	Width of helical PM (mm)	9.5
$h_{hm}$	Thickness of helical PM (mm)	4.5
$a_c$	Thickness of rotor inner core (mm)	5.5
$a_s$	Thickness of rotor outer core (mm)	10.5
$a_{sc}$	Thickness ratio of rotor outer core to inner core	1.91
$w_{em}$	Width of the excitation PM (mm)	22.5
$h_{em}$	Thickness of the excitation PM (mm)	6
$h_{so}$	Thickness of stator tooth tip (mm)	0.6
$h_{sl}$	Thickness of stator tooth transition section (mm)	0.4
$h_{s2}$	Length of stator teeth (mm)	10.5
$w_t$	Width of stator teeth (mm)	3.1
$b_s$	Width of stator slot opening (mm)	2.5

TABLE VI  
THE RANGE OF OPTIMIZATION PARAMETERS

Parameter	Variation range	Parameter	Variation range
$b_s$	[2.4 ~ 3.2] mm	$w_{hm}$	[7 ~ 10] mm
$w_t$	[2.5 ~ 3.4] mm	$h_{hm}$	[3 ~ 6] mm
$w_{em}$	[21 ~ 24] mm		

1  
2  
3 TEC-01067-2023  
4  
5

8

application.

5) *Winding Design*

The combination of 39 slots and 12 poles leads to asymmetry of the windings, which is manifested by the fact that the number of slots in a unit-motor set cannot be evenly divided by three phases. The slot pole combination has three sets of unit-motor according to the greatest common denominator of the number of slots and poles. The windings are corrected by arranging overlapping coils for one of the phases in each unit-motor unit. The winding arrangement is given in Fig. 15. The star diagrams of the slot electromotive force (EMF) of the three unit-motor sets and their syntheses are given in Fig. 17(a) and (b), respectively. The phase difference between the three-phase windings can be calculated from the slot EMF star diagrams as:

$$\begin{cases} \angle(A, B) = 117.39^\circ, \angle(A, C) = 123.42^\circ \\ \angle(B, C) = 119.19^\circ \end{cases} \quad (3a)$$

The maximum phase deviation of the asymmetrical winding is  $3.42^\circ$  compared to the symmetrical winding, which can be considered a more minor deviation. The overlapping coils are reflected in Fig. 15, and the dashed vectors in Fig. 17(a).

The winding coefficient  $K_w$  related to the distribution factor  $k_d$  and pitch factor  $k_p$  can be calculated as

$$\begin{cases} k_p = \sin\left(\frac{y_1}{\tau} 90^\circ\right) = 0.823, \quad k_d = \frac{\sin(q\alpha/2)}{q \sin(\alpha/2)} = 0.993 \\ K_w = k_p k_d = 0.817 \end{cases} \quad (3a)$$

where  $y_1$  is the pitch of the coil,  $\tau$  is the pole pitch,  $q$  is the number of slots per pole per phase, and  $\alpha$  is the slot pitch electrical angle.

4) *The results of the initial design*

Based on the rated parameters of the proposed LRWG given

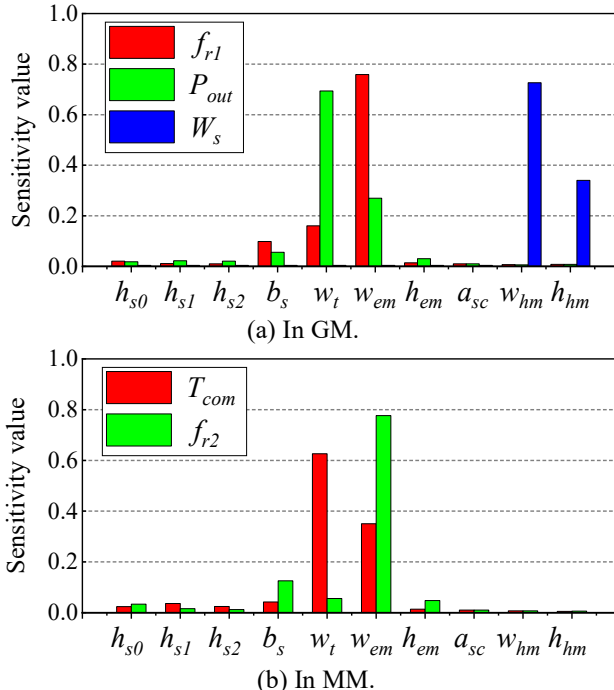


Fig. 19. Sensitivity analysis results.

in Table II, the initial design can be obtained and listed in Table III through the proposed design method. Some correlation coefficients, such as load and PM parameters, etc., are also included in Table III and IV.

## IV. MULTI-OBJECTIVE OPTIMIZATION AND EXPERIMENTAL VALIDATION

A. *Multi-objective Optimization Algorithm*

After completing the initial design, the proposed LRWG can basically satisfy the constraints of the rated parameters. However, torque ripple, harmonic distortion rate, shear torque, etc., also need to be considered, so the proposed LRWG is a multi-objective device. Therefore, a multi-objective optimization algorithm is required.

To improve the capture efficiency from the wave in the WEC system, the generator should occasionally operate in MM to implement a maximum power tracking strategy [17]. Therefore, a multi-mode, multi-objective optimization method is proposed, which can consider GM and MM, and its

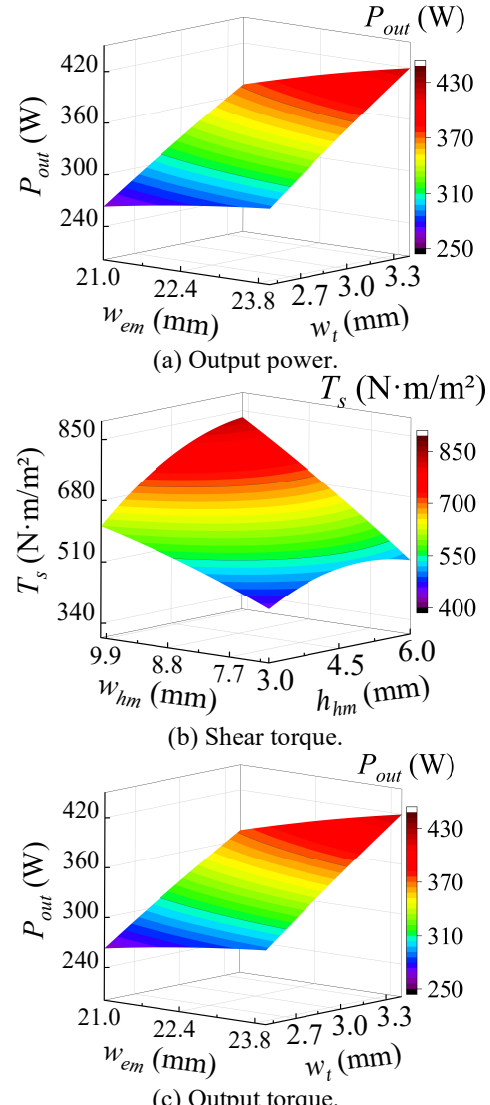


Fig. 20. RSM analysis results.

TEC-01067-2023

flowchart is shown in Fig. 16.

#### 1) Optimization Objectives and Constraints

The functions of the two operating modes of the proposed LRWG are different, so they have different optimization objectives.

##### a) Generator Mode:

The GM is the main operation mode, so the output power is determined as one of the optimization objectives. Due to the complexity of the wave, running steadily is necessary, so torque ripple is chosen as one of the optimization objectives. In addition, to increase the PM utilization, the shear torque is selected as another objective:

$$w_s = T_r / (2\pi r_a l_z) \quad (3a)$$

In summary, the optimization objectives and constraints can be expressed as:

$$\begin{cases} \text{Function : } [\max(P_{out}), \max(W_s), \min(f_{rl})] \\ \text{Constraint : } \begin{bmatrix} 0.8P_{rated} \leq P_{out} \leq 1.2P_{rated}, \\ W_s \geq W_i, f_{rl} \leq 20\%, f_{THD} \leq 15\% \end{bmatrix} \end{cases} \quad (3a)$$

where  $P_{out}$ ,  $P_{rated}$ ,  $f_{rl}$ , and  $f_{THD}$  are output power, rated power, torque ripple coefficient in GM, and harmonic distortion ratio of the induced voltage, respectively.  $T_s$  is the maximum shear torque, and  $W_i$  is the maximum shear torque corresponding to the initial design.

##### b) Motor Mode:

For the MM, the output torque and steadiness are essential, so the output compensation torque  $T_{com}$  and torque ripple are selected as the optimization objectives, which can be

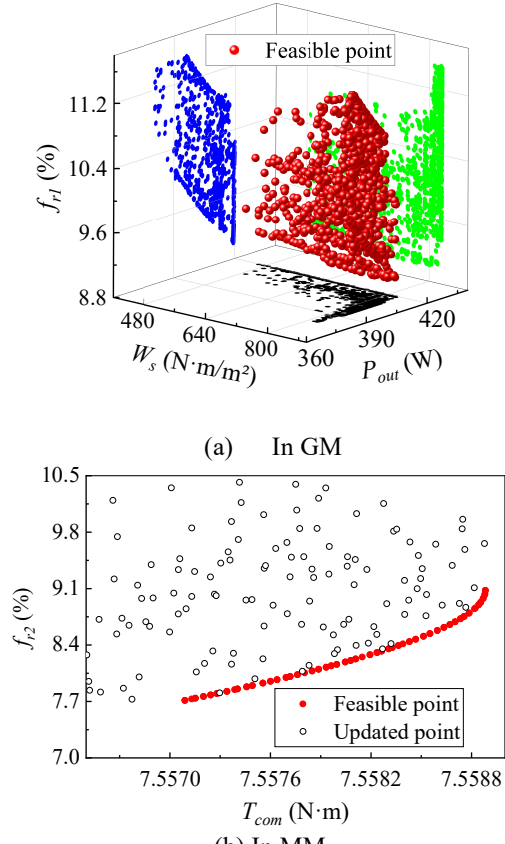


**Fig. 21.** Feasible solutions in two modes of operation.

expressed as:

$$\begin{cases} \text{Function : } [\max(T_{com}), \min(f_{r2})] \\ \text{Constraint : } [T_{com} \geq 0.9T_i, f_{r2} \leq 20\%] \end{cases} \quad (3a)$$

where  $f_{r2}$  is the torque ripple coefficient in MM and  $T_i$  is the output torque corresponding to the initial design.

#### 2) Sensitivity Analysis

Numerous design parameters can lead to significant time consumption, so it is essential to identify highly sensitive parameters in the optimization procedure by sensitivity analysis [18]-[21]. While ensuring that the basic dimensions remain constant, the main design parameters are given in Fig. 18, and their initial values are listed in Table V.

The sensitivity analysis results are shown in Fig. 19. It can be seen that  $b_s$ ,  $w_t$ ,  $w_{em}$ ,  $w_{hm}$ , and  $h_{hm}$  have a more significant impact on the performance of LRWG, so they are determined as optimization parameters entering the optimization program. Their ranges are given in Table VI.

#### 3) Optimization

The proposed LRWG has both linear and rotational motions, so only a three-dimensional finite element model can be established to analyze it, which consumes a lot of time if the finite element analysis is used directly to find the optimal value. Aiming at this problem, RSM is adopted to avoid extensive finite element calculations. Then, the optimal solutions in each operation mode are found by NSGA II [22].

The results of the RSM analysis of the output power  $P_{out}$  and maximum shear torque  $T_s$  in the GM and the output torque  $T_{com}$  in the MM are shown in Fig. 20. The feasible solutions in

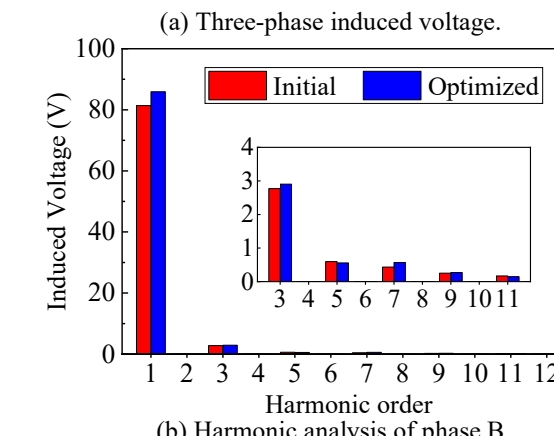
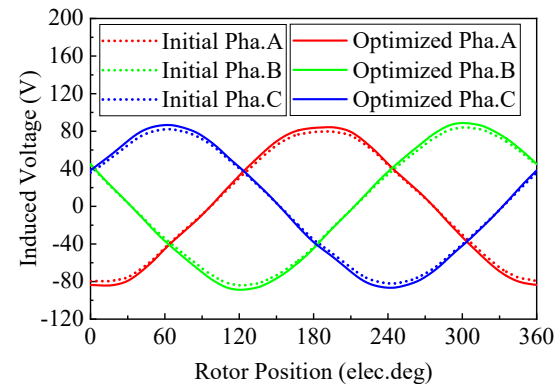


**Fig. 22.** Induced voltage and its harmonic analysis.

1  
2  
3 TEC-01067-2023  
4  
5  
6  
7  
8  
9  
10  
11  
12  
13  
14  
15  
16  
17  
18  
19  
20  
21  
22  
23  
24  
25  
26  
27  
28  
29  
30  
31  
32  
33  
34  
35  
36  
37  
38  
39  
40  
41  
42  
43  
44  
45  
46  
47  
48  
49  
50  
51  
52  
53  
54  
55  
56  
57  
58  
59  
60

two modes of operation are shown in Fig. 21, where each solution corresponds to a set of design parameter values.

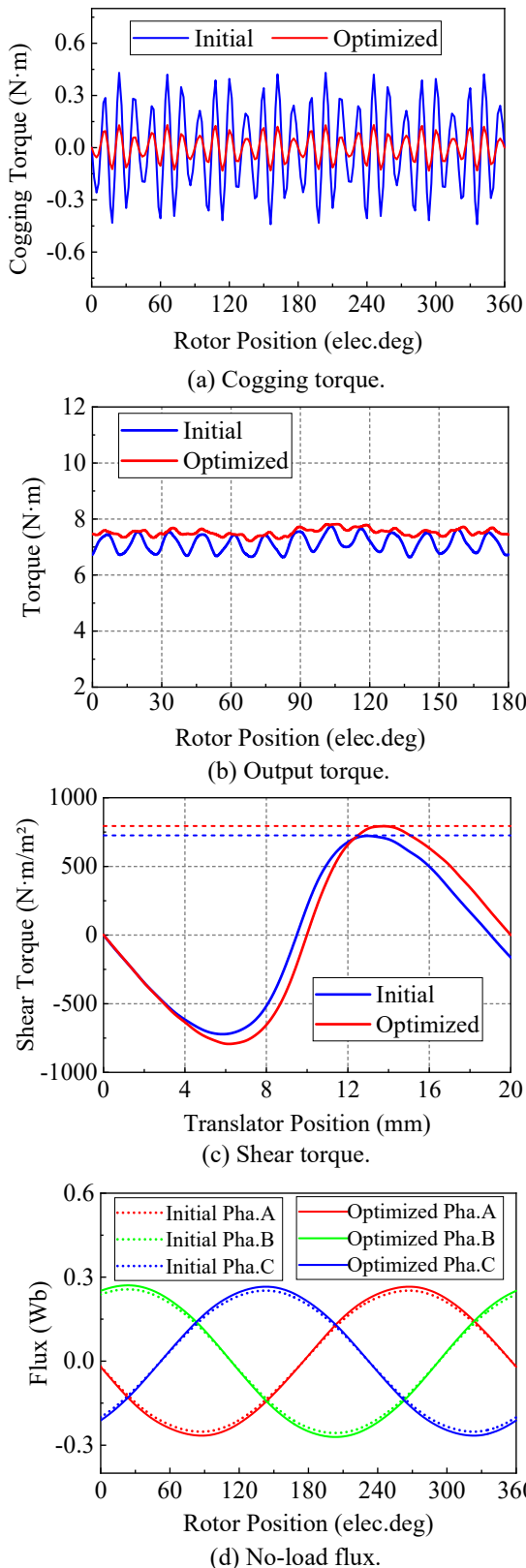


**Fig. 23.** Performance comparison of initial and optimized LRWGs.

#### 4) Final Value decision

The intersection of the feasible solutions in each operating mode determines the candidate designs. Then, the final optimal results are determined by the evaluation function. Combining the running time ratio of the two modes and the weight of the optimization objectives in each mode, the evaluation function is defined as

$$f_{\max} = \delta_1 \left( \frac{\varepsilon_1 P_{out}}{P_i} + \frac{\varepsilon_2 W_s}{W_i} + \frac{\varepsilon_3 f_{rl}}{f_{rl}} \right) + \delta_2 \left( \frac{\varepsilon_1 T_{com}}{T_i} + \frac{\varepsilon_2 f_{r2}}{f_{r2}} \right) \quad (3a)$$

where  $P_i$  is the output power corresponding to the initial design, and  $f_{rl}$  and  $f_{r2}$  are the torque ripple coefficients corresponding to the initial design, respectively, for the GM and MM.  $\delta_1$  and  $\delta_2$  are the weight coefficients of the two modes, which are 0.7 and 0.3, respectively, according to the running time of the two modes.  $\varepsilon_1$ ,  $\varepsilon_2$ , and  $\varepsilon_3$  are the weight coefficients of the corresponding optimization objectives in GM, which are 0.35, 0.35, and 0.3, respectively.  $\varepsilon_1$  and  $\varepsilon_2$  are the weight coefficients of the corresponding optimization objectives in MM, which are 0.65 and 0.35, respectively.

Application of the evaluation function (12) to the candidate designs resulted in the final design, given in Table VI, which

TABLE VII  
THE VOLUME AND MASS OF THE LRWG PROTOTYPE

Quantity (unit)	Value
Volume of the translator core ( $\text{cm}^3$ )	1549.06
Volume of the translator helical PM ( $\text{cm}^3$ )	631.15
Volume of the rotor helical PM ( $\text{cm}^3$ )	57.49
Volume of the rotor inner core ( $\text{cm}^3$ )	98.83
Volume of the rotor outer core ( $\text{cm}^3$ )	173.18
Volume of the excitation PM ( $\text{cm}^3$ )	101.52
Volume of the stator core ( $\text{cm}^3$ )	674.11
Volume of the winding coil ( $\text{cm}^3$ )	78.77
Mass of the translator core (kg)	12.16
Mass of the translator helical PM (kg)	4.70
Mass of the rotor helical PM (kg)	0.43
Mass of the rotor inner core (kg)	0.78
Mass of the rotor outer core (kg)	1.32
Mass of the excitation PM (kg)	0.76
Mass of the stator core (kg)	5.16
Mass of the winding coil (kg)	0.70

TABLE VIII  
THE INITIAL AND OPTIMIZED PARAMETERS COMPARISON

	Initial	Optimized		Initial	Optimized
$b_s$	2.5	2.5989	$w_{hm}$	9.5	9.9939
$w_t$	3.1	3.2996	$h_{hm}$	4.5	5.0802
$w_{em}$	22.5	23.4974			

TABLE IX  
THE PERFORMANCE OPTIMIZATION RESULTS

Mode	Item (unit)	Initial	Optimized
GM	$P_{out}$ (W)	357.88	398.92
	$W_s$ ( $\text{N}\cdot\text{m}/\text{m}^2$ )	738.77	791.76
	$f_{rl}$ (%)	14.77	8.98
MM	$T_{com}$ ( $\text{N}\cdot\text{m}$ )	7.14	7.53
	$f_{r2}$ (%)	16.22	8.61

1  
2  
3 TEC-01067-2023  
4  
5

11

also contains the objective values corresponding to the final design compared to the initial design.

#### B. Application of the Proposed Optimization Algorithm

An initial design proposal in Table III is applied to the proposed optimization algorithm. The structure parameters and performance results between the initial and optimized results are compared in Tables VIII and IX. The results show that all performance is improved under both the GM and MM. The initial and optimal results comparison of the EMF is given in Fig. 22. Compared to the initial design, the amplitude is slightly increased.

The comparison results of the cogging, output, and shear torque are given in Fig. 23, and they are both improved. Also, the no-load flux is improved as shown in Fig. 23(d).

The flux density distribution of ET and EC are shown in Fig. 26 under the rated operation condition. From the figure, the saturation effect does not appear on the translator and common rotor. That's because a large redundancy is given at the initial design process considering the ocean application.

#### C. Experimental Verification

##### 1) Prototype and Experimental Platform

To further validate the feasibility of the proposed LRWG, the prototype was manufactured based on the optimization

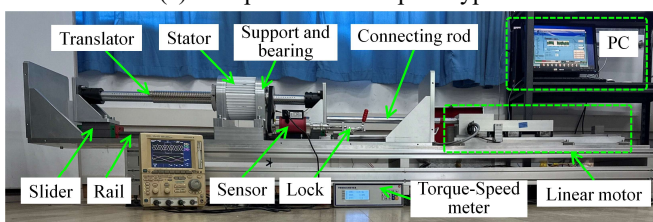
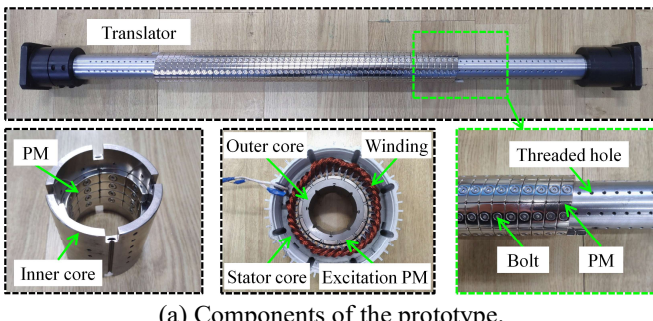


**Fig. 24.** LRWG prototype and experimental platform.

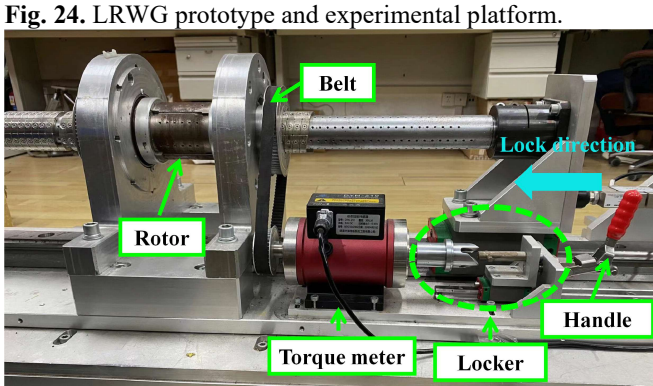


**Fig. 25.** The Locker

results, as shown in Fig. 24(a), and its experimental platform was built, as shown in Fig. 24(b). The volume and mass parameters of the LRWG prototype are given, as shown in Table VII. A linear motor is adopted as a driver to simulate wave motion for the LRWG. And they are connected by a connecting rod. The translator is mounted on a linear guide utilizing the slider to ensure it moves in a straight line. The rotor is fixed between the supports utilizing rolling bearings, and the supports are provided with bulges supporting the stator.

##### 2) Performance Test for ET Section

The static thrust force and torque of the ET section were tested when the rotor was locked. A synchronous belt connects the rotor to the torque-speed sensor. When the linear motor drives the translator to move, the rotor torque can be measured from the torque speed sensor, and the measured thrust force of the translator can be obtained through the linear motor controller. The rotor is locked by a locker as shown in Fig. 25, which is mechanically connected with the torque meter and rotor. When the torque meter is fixed by the locker, the rotor also be fixed through the belt simultaneously. The measured thrust force and torque results are shown in Fig. 27, compared

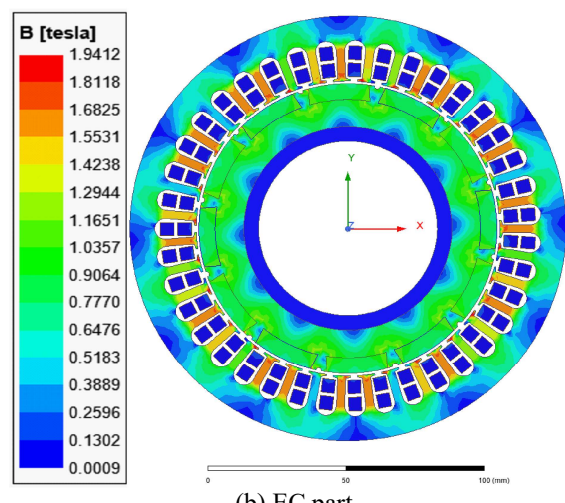
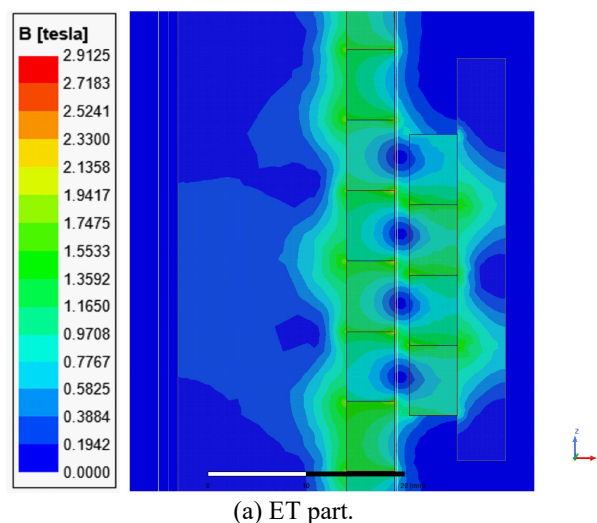


**Fig. 26.** The flux density distribution of the optimized LRWG.

1  
2  
3  
4  
5  
6  
7  
TEC-01067-2023

12

with finite element simulations. The maximum thrust force and torque errors are 5.94% and 8.62% from the results, respectively.

### 3) No-load and Load Testing

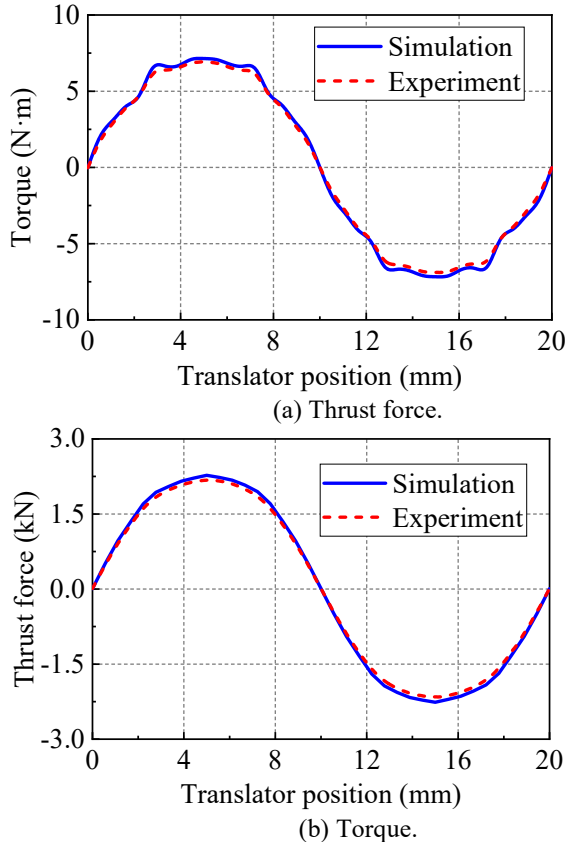


Fig. 27. Results of force performance test for ET section.

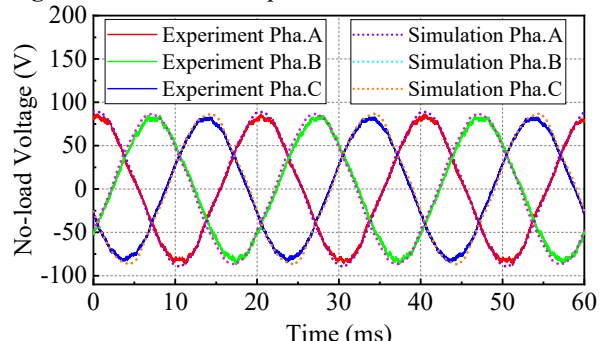


Fig. 28. Experimental no-load voltage.

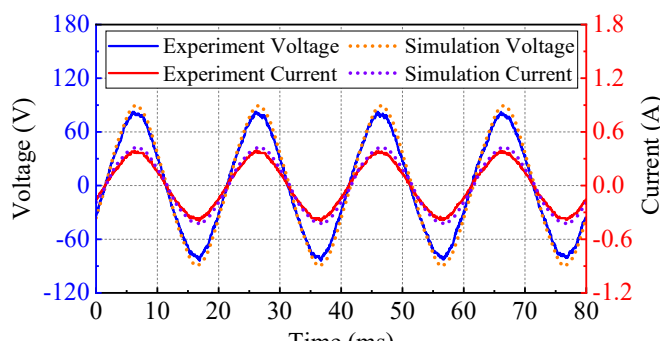


Fig. 29. Experimental load voltage and current.

Firstly, the experiment was carried out with no load. The translator runs at a rated speed of 0.1667 m/s, and the rotor runs at a rated speed of 500 rpm through the ET section transmission. The experimental three-phase no-load voltages are shown in Fig. 28 and compared with the finite element simulations. There is good agreement between the two types of results. The experimental and simulated amplitudes are 84.21 V and 88.57 V, respectively.

Then, a three-phase Y-connected resistive load was connected for load testing, where the resistance is 200  $\Omega$ . The rotor also runs at rated speed. The experimental voltage and current of one of the phases compared with the simulation are given in Fig. 29. The amplitude of the experimental voltage and current are 82.42 V and 0.38 A, respectively, and the amplitude of voltage and current obtained by simulation are 89.07 V and 0.42 A, respectively.

## V. CONCLUSION

A novel direct-driven LRWG is proposed in this paper, which can increase the power density by converting the low-speed linear motion into high-speed rotating motion. The proposed LRWG comprises three parts: translator, common rotor, and stator. The common rotor core is divided into two layers by two different materials, which simultaneously function for energy transmission and conversion.

An initial design method, which can consider both the ET and EC sections, is proposed first. To improve the reliability of the moving parts, the rotor core was divided into a two-layer structure of carbon steel and silicon steel, and its feasibility was analyzed. A bolt fixing method was adopted to solve the problem of mounting accuracy of the PM segments, and the effects of the hole radius of the PM and the bolt material on the force performance were analyzed.

Then, a multi-mode and multi-objective optimization method is proposed, considering both GM and MM. And the feasibility of the optimization method is verified by the FEM.

Finally, a prototype of the proposed LRWG with its experimental platform was developed based on the optimization results. The force/torque performance of the ET section was tested, and no-load and load experiments were performed. The results between the experimental and FEM are compared, and the experiment verifies the effectiveness of the FEM.

## REFERENCES

- [1] S. Rasool, K. M. Muttaqi and D. Sutanto, "A Multi-Filter Based Dynamic Power Sharing Control for a Hybrid Energy Storage System Integrated to a Wave Energy Converter for Output Power Smoothing," *IEEE Trans. Sustain. Energy*, vol. 13, no. 3, pp. 1693-1706, July 2022, doi: 10.1109/TSTE.2022.3170938.
- [2] N.Y. Sergienko, B.S. Cazzolato, B. Ding, and M. Arjomandi, "An optimal arrangement of mooring lines for the three-tether submerged point-absorbing wave energy converter," *Renew. Energy*, vol. 93, pp. 27-37, Aug. 2016, doi: 10.1016/j.renene.2016.02.048.
- [3] Z. Nie, X. Xiao, R. McMahon, P. Clifton, Y. Wu and S. Shao, "Emulation and Control Methods for Direct Drive Linear Wave Energy Converters," *IEEE Trans. Ind. Inf.*, vol. 9, no. 2, pp. 790-798, May 2013, doi: 10.1109/TII.2012.2224120.
- [4] M. Shadman, G. O. G. Avalos, S. F. Estefen, "On the power performance of a wave energy converter with a direct mechanical drive power take-off system controlled by latching," *Renew. Energy*, vol. 169, pp. 157-177, May 2021, doi: 10.1016/j.renene.2021.01.004.

1  
2  
3 TEC-01067-2023  
4  
5  
6  
7  
8  
9  
10  
11  
12  
13  
14  
15  
16  
17  
18  
19  
20  
21  
22  
23  
24  
25  
26  
27  
28  
29  
30  
31  
32  
33  
34  
35  
36  
37  
38  
39  
40  
41  
42  
43  
44  
45  
46  
47  
48  
49  
50  
51  
52  
53  
54  
55  
56  
57  
58  
59  
60

- [5] Y. Gao, S. Shao, H. Zou, M. Tang, H. Xu, and C. Tian, "A fully floating system for a wave energy converter with direct-driven linear generator," *Energy*, vol. 95, pp. 99-109, Jan 2016, doi: 10.1016/j.energy.2015.11.072.
- [6] S. Meng, Z. Ling, W. Zhao, J. Ji and M. Xu, "Design and Analysis of a Surface-inserted Magnetic Screw With Minimum Thrust Force Ripple," in *IEEE Transactions on Transportation Electrification*, doi: 10.1109/TTE.2024.3349530.
- [7] L. Zhu et al., "A Novel Hybrid Excitation Magnetic Lead Screw and Its Transient Sub-Domain Analytical Model for Wave Energy Conversion," in *IEEE Transactions on Energy Conversion*, doi: 10.1109/TEC.2024.3354512.
- [8] Z. Ling, J. Ji, J. Wang, and W. Zhao, "Design Optimization and Test of a Radially Magnetized Magnetic Screw With Discretized PMs," *IEEE Trans. Ind. Electron.*, vol. 65, no. 9, pp. 7536-7547, Sept. 2018, doi: 10.1109/TIE.2017.2740820.
- [9] H. Wang et al., "A New Wave Energy Converter for Marine Data Buoy," *IEEE Trans. Ind. Electron.*, vol. 70, no. 2, pp. 2076-2084, Feb. 2023, doi: 10.1109/TIE.2022.3159917.
- [10] C. S. Cyusa and Y. Fujimoto, "Enactment-Based Direct-Drive Test of a Novel Radial-Gap Helical RotLin Machine," *IEEE Trans. Ind. Appl.*, vol. 54, no. 2, pp. 1273-1282, March-April 2018, doi: 10.1109/TIA.2017.2766578.
- [11] Z. Ling, W. Zhao, P. O. Rasmussen, J. Ji, Y. Jiang and Z. Liu, "Design and Manufacture of a Linear Actuator Based on Magnetic Screw Transmission," *IEEE Trans. Ind. Electron.*, vol. 68, no. 2, pp. 1095-1107, Feb. 2021, doi: 10.1109/TIE.2020.2967731.
- [12] Z. Liu and J. Wang, "Design and testing of a high force density linear electromagnetic actuator," 2020 IEEE Energy Conversion Congress and Exposition (ECCE), Detroit, MI, USA, 2020, pp. 1145-1152, doi: 10.1109/ECCE44975.2020.9236128.
- [13] L. Xu, X. Zhu, C. Zhang, L. Zhang and L. Quan, "Power Oriented Design and Optimization of Dual Stator Linear-Rotary Generator With Halbach PM Array for Ocean Energy Conversion," *IEEE Trans. Energy Convers.*, vol. 36, no. 4, pp. 3414-3426, Dec. 2021, doi: 10.1109/TEC.2021.3070633.
- [14] L. Zhu, Q. Wu, W. Li, W. Wu, C. -s. Koh and F. Blaabjerg, "A Novel Consequent-Pole Magnetic Lead Screw and Its 3-D Analytical Model with Experimental Verification for Wave Energy Conversion," in *IEEE Transactions on Energy Conversion*, doi: 10.1109/TEC.2023.3331008.
- [15] L. Li and G. Zhu, "Electromagnetic-Thermal-Stress Efforts of Stator-Casing Grease Buffers for Permanent Magnet Driving Motors," in *IEEE Transactions on Industry Applications*, vol. 60, no. 1, pp. 1268-1276, Jan.-Feb. 2024, doi: 10.1109/TIA.2023.3291680.
- [16] K. Jenney and S. Pakdelian, "Magnetic Design Aspects of the Trans-Rotary Magnetic Gear Using Quasi-Halbach Arrays," *IEEE Trans. Ind. Electron.*, vol. 67, no. 11, pp. 9582-9592, Nov. 2020, doi: 10.1109/TIE.2019.2955424.
- [17] C. Wei, Z. Zhang, W. Qiao and L. Qu, "Reinforcement-Learning-Based Intelligent Maximum Power Point Tracking Control for Wind Energy Conversion Systems," *IEEE Trans. Ind. Electron.*, vol. 62, no. 10, pp. 6360-6370, Oct. 2015, doi: 10.1109/TIE.2015.2420792.
- [18] X. Sun, N. Xu and M. Yao, "Sequential Subspace Optimization Design of a Dual Three-Phase Permanent Magnet Synchronous Hub Motor Based on NSGA III," *IEEE Trans. Transp. Electrif.*, vol. 9, no. 1, pp. 622-630, March 2023, doi: 10.1109/TTE.2022.3190536.
- [19] G. Du, N. Huang, Y. Zhao, G. Lei and J. Zhu, "Comprehensive Sensitivity Analysis and Multiphysics Optimization of the Rotor for a High Speed Permanent Magnet Machine," *IEEE Trans. Energy Convers.*, vol. 36, no. 1, pp. 358-367, March 2021, doi: 10.1109/TEC.2020.3005568.
- [20] Z. Shi et al., "Design Optimization of a Spoke Type Axial-Flux PM Machine for In-wheel Drive Operation," in *IEEE Transactions on Transportation Electrification*, doi: 10.1109/TTE.2023.3310738.
- [21] Z. Shi, X. Sun, Y. Cai and Z. Yang, "Robust Design Optimization of a Five-Phase PM Hub Motor for Fault-Tolerant Operation Based on Taguchi Method," *IEEE Trans. Energy Convers.*, vol. 35, no. 4, pp. 2036-2044, Dec. 2020, doi: 10.1109/TEC.2020.2989438.
- [22] X. Sun, Z. Shi, G. Lei, Y. Guo and J. Zhu, "Multi-Objective Design Optimization of an IPMSM Based on Multilevel Strategy," *IEEE Trans. Ind. Electron.*, vol. 68, no. 1, pp. 139-148, Jan. 2021, doi: 10.1109/TIE.2020.2965463.



**Lixun Zhu** (Member, IEEE) received his Ph. D. degree in electrical engineering from Chungbuk National University, Korea in 2018. He is an associate professor in the Department of Electrical Engineering at Shanghai Maritime University, China.

His research interests include wave energy conversion, motor design, and iron loss modeling.



**Lei Zhu** was born in Kunshan, Jiangsu Province, China 2000. He is currently working toward the M.S. degree in the department of electrical engineering, Shanghai Maritime University, China.

His research interests include the optimization of a novel wave generator.



**Qingyun Wu** was born in Henan, China. He is currently working toward the M.S. degree in the department of electrical engineering, Shanghai Maritime University, China.

His research interests include analytical modeling of magnetic lead screws and design and optimization of a novel wave generator.



**Ting Xu** was born in Zhejiang, China. He graduated with an M.S. degree in Electrical Engineering from Washington University in St. Louis after earning his bachelor's degree from Shanghai Maritime University, China. His research interests lie in optimization methodologies and computational techniques, including machine learning algorithms to enhance the design and performance of complex engineering systems.



**Wei Li** (Member, IEEE) was born in Suihua, China. She received her B.S. and M.S. degrees in electrical engineering from Harbin Institute of Technology, Harbin, China, in 2005 and 2007, respectively. She received her Ph. D. degree in electrical engineering from Chungbuk National University, Chungbuk, Korea, in 2011.

She has been an assistant professor at the School of Electronics and Information Engineering at Tongji University, Shanghai, China, since 2012. She is now an associate professor at Tongji University. Her current research interests include hysteresis modeling, finite element method, partial

1  
2 TEC-01067-2023  
3  
4  
5  
6  
7  
8  
9  
10  
11  
12  
13  
14  
15  
16  
17  
18  
19  
20  
21  
22  
23  
24  
25  
26  
27  
28  
29  
30  
31  
32  
33  
34  
35  
36  
37  
38  
39  
40  
41  
42  
43  
44  
45  
46  
47  
48  
49  
50  
51  
52  
53  
54  
55  
56  
57  
58  
59  
60

element equivalent method and their applications, control of electrical machines, and so on.



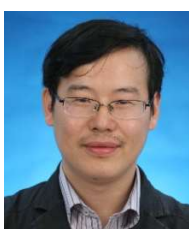
**Min Huang** (Member, IEEE) received the M.S. degree in electrical engineering from Shanghai Maritime University, Shanghai, China, in 2012, and the Ph.D. degree from the Institute of Energy Technology, Aalborg University, Aalborg, Denmark, in 2015. She is currently a Faculty Member at Shanghai Maritime University. Her research interests include power quality, control, and power converters for renewable energy systems.



**Ning Gao** (Member, IEEE) was born in Haining, Zhejiang Province, China 1987. He received his B.S. degree in electronics and information engineering from Zhejiang University, Hangzhou, China, in 2009, and his M.S. and Ph.D. degrees from Shanghai Jiao Tong University, Shanghai, China, in 2011 and 2017, respectively. Since 2017, he has been with the Department of Electrical Engineering, Shanghai Maritime University, Shanghai, where he is currently an Assistant Professor. His research interests mainly include control strategies and topologies of power converters applied in battery energy storage systems.



**Kangan Wang** received the B.S. and Ph.D. degrees in electrical engineering from China University of Mining and Technology, Xuzhou, China, in 2013 and 2019, respectively. Since 2020, he has been with Logistics Engineering College, Shanghai Maritime University. His research interests include power electronic-based smart transformers, cascaded H-bridge converters, and dc-dc converters.



**Weimin Wu** (Member, IEEE) received a Ph.D. degree in electrical engineering from the College of Electrical Engineering, Zhejiang University, Hangzhou, China, in 2005.

From July 2005 to June 2006, he was a Research Engineer with the Delta Power Electronic Center in Shanghai, China. Since July 2006, he has been a Faculty Member at Shanghai Maritime University, Shanghai, China, where he is a Full Professor in the Department of Electrical Engineering. From September 2008 to March 2009, he was a visiting professor at the Center for Power Electronics Systems, Virginia Polytechnic Institute and State University, Blacksburg, VA, USA. From November 2011 to January 2014, he was also a Visiting Professor with the Department of Energy Technology,

Aalborg University, Aalborg, Denmark, working with the Center of Reliable Power Electronics. He has co-authored more than 180 papers and holds eight patents. His research interests include power converters for renewable energy systems, power quality, smart grid, and energy storage technology.

Dr. Wu is currently an Associate Editor for the IEEE TRANSACTIONS ON INDUSTRY ELECTRONICS.



**Chang-Seop Koh** (Senior Member, IEEE) received the B.S., M.S., and Ph.D. degrees in electrical engineering from Seoul National University, Seoul, South Korea, in 1982, 1986, and 1992, respectively.

Since 1996, he has been a Professor at the College of Electrical and Computer Engineering, Chungbuk National University, Cheongju, South Korea. His research interests include numerical methods for electromagnetic field analysis, design optimization of electromagnetic devices, and measurement of magnetic properties of silicon steel.



**Frede Blaabjerg** (Fellow, IEEE) received the Ph.D. degree in electrical engineering from Aalborg University, Copenhagen, Denmark, in 1995, and the Honoris Causa degree from University Politehnica Timisoara, Timisoara, Romania, and Tallinn Technical University, Tallinn, Estonia.

From 1987 to 1988, he was with ABB-Scandia, Randers, Denmark. He became an Assistant Professor in 1992, Associate Professor in 1996, and a Full Professor of Power Electronics and Drives in 1998. Since 2017, he has been a Villum Investigator. He has authored or coauthored more than 600 journal papers in the fields of power electronics and its applications. He is also the coauthor of four monographs and editor of ten books in power electronics and its applications. His current research interests include power electronics and its applications such as in wind turbines, PV systems, reliability, harmonics, and adjustable speed drives.

Dr. Blaabjerg was the recipient of the 32 IEEE Prize Paper Awards, IEEE PELS Distinguished Service Award in 2009, EPE-PEMC Council Award in 2010, IEEE William E. Newell Power Electronics Award 2014, Villum Kann Rasmussen Research Award 2014, Global Energy Prize in 2019 and the 2020 IEEE Edison Medal. He was the Editor-in-Chief of IEEE TRANSACTIONS ON POWER ELECTRONICS from 2006 to 2012. He has been a Distinguished Lecturer for the IEEE Power Electronics Society, from 2005 to 2007, and for the IEEE Industry Applications Society from 2010 to 2011, and 2017 to 2018. During 2019–2020, he was the President of IEEE Power Electronics Society. He is also the Vice-President of the Danish Academy of Technical Sciences Lyngby, Denmark. He is nominated in 2014–2021 by Thomson Reuters to be between the most 250 cited researchers in Engineering in the world.